



# Probabilistic Stability Analysis of a Tunnel Face in Spatially Random Hoek–Brown Rock Masses with a Multi-Tangent Method

Tianzheng Li<sup>1</sup> · Qiuqing Pan<sup>2</sup> · Zhichao Shen<sup>3</sup> · Wenping Gong<sup>1</sup>

Received: 22 June 2021 / Accepted: 16 February 2022 / Published online: 9 March 2022  
© The Author(s), under exclusive licence to Springer-Verlag GmbH Austria, part of Springer Nature 2022

## Abstract

Tunnel excavations in heavily fractured rock masses are often subjected to the high risk of face instability. To solve this problem, the probabilistic stability analysis of tunnel face is performed in this contribution, in which the fractured rock masses are modelled as spatially random media that follow the Hoek–Brown failure criterion. The method of Karhunen–Loève expansion is adopted to characterize the spatial variabilities of Hoek–Brown parameters. Under this circumstance, the conventional tangent technique fails to integrate the Hoek–Brown failure criterion into the kinematical approach of limit analysis framework. Thus, the multi-tangent method which permits to use multiple tangent lines to represent the nonlinear Hoek–Brown failure envelope is proposed. A discretized three-dimensional failure mechanism of tunnel face is adopted to determine critical face pressures within the framework of limit analysis. Due to a large number of input variables required by the generation of random fields, the global sensitivity analysis and a sparsity scheme are employed to reduce the problem dimension. The method of sparse polynomial chaos expansion is then employed to perform Monte Carlo simulation with a significant reduction of calls to the computationally expensive original model. Finally, the parametric analysis on the deterministic model and probabilistic model is performed to gain an insight into the proposed approach.

## Highlights

- The three-dimensional stability of a tunnel face driven in Hoek-Brown rock masses is evaluated by combining the limit analysis and random field theory.
- The method of Karhunen-Loève expansion is adopted to characterize the spatial variabilities of Hoek-Brown parameters.
- A multi-tangent method is proposed to determine the equivalent shear strength parameters of rock masses.
- A fast and accurate probabilistic model for tunnel face reliability analysis is obtained with the sparse polynomial chaos expansion method.

**Keywords** Probabilistic stability analysis · Hoek–Brown failure criterion · Random field · Multi-tangent method · Spare polynomial chaos expansion

✉ Qiuqing Pan  
qiuqing.pan@csu.edu.cn

✉ Zhichao Shen  
shenzhch@163.com

<sup>1</sup> Faculty of Engineering, China University of Geosciences,  
Wuhan 430074, China

<sup>2</sup> School of Civil Engineering, Central South University,  
Hunan 410075, China

<sup>3</sup> Department of Civil and Environmental Engineering,  
National University of Singapore, Singapore 117576,  
Singapore

## List of symbols

$\sigma_1$	Maximum principle stress
$\sigma_3$	Minimum principle stress
$\sigma_c$	Uniaxial compressive strength
$m_i$	Constant related to the hardness of the rock masses
GSI	Geological strength index
$D$	Artificial disturbance factor
$c_t$	Equivalent cohesion of rock masses
$\varphi_t$	Equivalent internal friction angle of rock masses
$G_i$	Lognormal random field of parameter $i$
$G_{lni}$	Normal random field of parameter $lni$
$\mu_i$	Mean value of parameter $i$

$\sigma_i$	Standard deviation of parameter $i$
$M$	Number of truncation terms in Karhunen–Loève expansion
$\xi_j$	Independent variable of standard normal distribution
$\lambda_j$	Eigenvalue of the autocorrelation function
$\psi_j$	Eigenfunction of the autocorrelation function
$\varepsilon_{err}$	Error of the Karhunen–Loève expansion
$\Omega$	Domain of the random field
$\rho_i$	Autocorrelation function
$\rho_{i,j}$	Cross-correlation between random fields of $i$ and $j$
$\theta_h$	Horizontal autocorrelation distance
$\theta_v$	Vertical autocorrelation distance
COV	Coefficient of variation
$\omega$	Angular velocity of the failure mechanism
$O$	Rotation center
$E$	Center of the circular tunnel face
$r_E$	Length of $OE$
$\beta_E$	Rotation angle of $OE$
$d$	Tunnel diameter
$\delta$	Side length of discretized element
$[\sigma_3]_n$	Minimum principle stress of the element $n$
$\gamma$	Unit weight of rock masses
$l$	Number of layers in the domain $\Omega$
$h_n$	Burial depth of the element $n$
$F$	Computational model
$Y$	Model response
$L$	Number of input variables
$\Psi_\alpha$	Multivariate polynomial
$\eta_j$	Unknown coefficients of the PCE
$P$	Number of terms in the truncated PCE
$H_\alpha$	Univariate polynomial
$\alpha$	Degree of the univariate polynomial
$p$	PCE order
$\ \alpha\ _q$	$q$ -Quasi-norm of $\alpha$
$\chi$	Experimental design
$N$	Size of experimental design
$\Psi$	Space-independent matrix with dimensions of $N \times P$
$S$	Sobol's indices
$R^2$	Coefficient of determination
$\varepsilon_{cut}$	Cutoff value:
$Q_{tgt}^2$	Target accuracy
$p_{max}$	Maximum PCE order
$g_T$	Performance function
$\sigma_U$	Applied face pressure
$\sigma_T$	Critical face pressure
$N_{MCS}$	Size of MCS population
$I$	Indicator function
$P_f$	Failure probability

## 1 Introduction

As tunnels often serve as important hubs of the highway or railway traffic, their safe and fast advancements are the guarantee of the whole project. However, tunnel constructions often encounter problems such as floor heave, surrounding rock instability, tunnel roof collapse and excavating face failure. Among these issues, the tunnel face failure has attracted much attention from scholars in the geotechnical engineering field. The kinematical approach of limit analysis is considered as an efficient way to assess the stability of tunnel face whose basic idea is to construct a work-balance equation in terms of the internal energy dissipation and the external work rate in a kinematically admissible velocity field. The critical face pressure is equal to the one that brings the tunnel face to the ultimate limit state. Early studies considered the failure mechanism of tunnel face to be composed of several blocks. When tunnel collapses, the blocks move toward the inside of the tunnel according to a translational velocity field. Leca and Dormieux (1990) used one or two truncated conical blocks to describe the three-dimensional (3D) tunnel face failure. Subsequently, Mollon et al. (2009) extended this failure mechanism into a multi-block one where the number of blocks was determined by an optimization process. Meanwhile, a spatial discretization technique was proposed to generate the 3D failure surface using a “point by point” method. The extended failure mechanism showed a great advantage due to its ability to cover the entire circular tunnel face and give a strict estimation of critical face pressures. Mollon et al. (2011a) presented a 3D rotational failure mechanism for stability analysis of a pressurized tunnel face in combination with the spatial discretization technique. This method seems more convincing since it does not require pre-setting the shape of the failure mechanism and takes into account the entire circular tunnel face instead of an inscribed ellipse to this circular area. Up to now, this method has been successfully used to assess the tunnel face stability in soils or fractured rock masses and proves to be an efficient way for quick estimations of critical face pressures in practical tunnel designs (Sun et al. 2018; Li et al. 2021).

In recent years, tunnel face stability in weak rock masses has become a hot topic due to the large-scale infrastructure construction undertaken in developing countries. Hoek and Brown (1980) proposed the original version of Hoek–Brown failure criterion. After several revisions and additions, the state-of-the-art Hoek–Brown failure criterion is available for stability analysis of rock structures, such as rock slopes, underground caves and tunnels (Hoek and Brown 1997; Hoek et al. 2002). Saada et al. (2013) performed the pseudo-static analysis of tunnel face stability in Hoek–Brown rock

masses. The influence of seismic loadings is taken into consideration. Pan and Dias (2018) presented a probabilistic approach for face stability of a rock tunnel by using polynomial chaos expansion (PCE) method. Luo and Yang (2018) proposed the analytical solution to stability of shallow tunnel roof with arbitrary profile under pore water pressure.

However, those studies treated the rock masses as a homogeneous medium while the properties of real rock masses are always spatially varying. Previously published works show that the spatial variability of geomaterials has a significant influence on geotechnical structures (Zhang and Goh 2012; Jiang et al. 2015; Yang and Wang 2011). Fenton and Griffiths (2003) presented an approach to predict the bearing capacity of a footing composed of spatially random cohesive-frictional soils. Pan and Dias (2017) performed the probabilistic stability analysis of tunnel face in spatially random soils, which is simulated by Karhunen–Loève (K–L) expansion. Guo et al. (2019) investigated the failure probability of the support lining of a shallow circular tunnel considering soil spatial variability. Traditional opinion holds that intact rock can be considered a homogeneous medium. However, for heavily fractured rock masses, the spatial variability of rock properties probably has a significant influence on the stability of a rock structure. Sow et al. (2017) proposed a methodology for analyzing the spatial variability of shear strength along the joints of rock mass, and a case study involving the sliding stability of a rock dam was presented. Chen et al. (2019) calculated the failure probability of crossing tunnels considering the spatial variability of rock property where the numerical package FLAC3D was adopted as a deterministic computational model.

Although face stability assessment for tunnels excavated in Hoek–Brown rock masses have been reported in many studies, few attempts have been made to address the influence of spatial variabilities of Hoek–Brown parameters. For this purpose, an efficient method is developed for the failure probability assessment of a rock tunnel face considering the spatial variabilities of Hoek–Brown parameters. The 3D rotational failure mechanism proposed by (Mollon et al. 2011a) is introduced to construct the deterministic computational model. The sparse polynomial chaos expansion (SPCE) proposed by (Blatman and Sudret 2010, 2011) is employed to assess the failure probability of tunnel face. The innovation of presented methodology is mainly reflected in the following four aspects: (1) the Hoek–Brown parameters are modeled as spatially random variables by means of the random field theory; (2) the multi-tangent method is proposed to integrate the nonlinear Hoek–Brown failure criterion into the kinematical approach of limit analysis; (3) the multi-tangent line method allows the rock masses at different locations to have different shear strength parameters according to their Hoek–Brown parameters and the stress state; (4) a SPCE-based surrogate model

is constructed for probabilistic analysis with a significant reduction of calls to the computationally expensive original model. Thanks to its efficient computing capability, the proposed method can be used as a tool for tunnel face stability analysis with a wide range of parameters. The obtained design charts or results can give much convenience and practicality in guiding engineering design and fast safety assessment.

## 2 Face Stability in Spatially Random Hoek–Brown Rock Masses

### 2.1 Hoek–Brown Failure Criterion and Multi-Tangent Method

The nonlinear Hoek–Brown failure criterion is extensively used to characterize the failure behavior of intact rock and heavily fractured rock masses (Renani and Martin 2020; Michalowski and Park 2020). The tangent technique is commonly used to extend the Hoek–Brown failure criterion into the kinematical approach of limit analysis (Yang and Yin 2010; Huang et al. 2021). This method uses a single tangent line to represent the uniform stress distribution along the entire failure surface; however, it fails to consider that the stress distribution along the failure surface is not uniform, due partly to the spatial variability of rock properties and partly to the variation of burial depth of tunnels. To solve this issue, the multi-tangent method is introduced. The principle idea is to use different tangent lines of the Hoek–Brown failure envelope to characterize the strength of rock masses at different locations. On this basis, the equivalent cohesions and equivalent internal friction angles at the failure surfaces can be obtained for the subsequent optimization calculations (Dadashzadeh et al. 2017).

Before introducing the multi-tangent method, we first review the Hoek–Brown failure criterion which takes the form of

$$\sigma_1 = \sigma_3 + \sigma_c \left( m \frac{\sigma_3}{\sigma_c} + s \right)^a, \tag{1}$$

where  $\sigma_1$  and  $\sigma_3$  denote the maximum and minimum principal stresses, respectively;  $\sigma_c$  refers to the uniaxial compressive strength of rock masses. The parameters of  $m$ ,  $s$  and  $n$  are expressed as

$$m = m_i \exp \left( \frac{GSI - 100}{28 - 14D} \right), \tag{2}$$

$$s = \exp \left( \frac{GSI - 100}{9 - 3D} \right), \tag{3}$$

$$a = \frac{1}{6} \left[ \exp\left(-\frac{GSI}{15}\right) - \exp\left(-\frac{20}{3}\right) \right] + \frac{1}{2}, \tag{4}$$

where  $m_i$  represents the hardness of the rock mass ranging between 1 and 35;  $GSI$  indicates the geological strength index changing from 5 for heavily fractured rock masses to 100 for intact rock;  $D$  is the artificial disturbance factor which is suggested to take 0 for tunnels driven by the tunnel boring machine (TBM) due to its limited disturbance to the nearby rock masses. In the framework of limit analysis, the nonlinear Hoek–Brown criterion often involves the work rate computations in the form of a pair of equivalent parameters, namely the equivalent cohesion  $c_t$  and the equivalent internal friction angle  $\varphi_t$ . Hoek et al. (2002) presents a strategy to cut the strength envelope of rock masses in the normal-shear stress plane using a straight line whose intercept on shear stress axis and inclination are considered as  $c_t$  and  $\varphi_t$ . However, this practice fails to yield the strict upper-bound solution because the strength of rock masses determined by a secant line can be smaller than the one by the convex envelope. To solve this issue, researchers replaced the nonlinear strength envelope with tangent lines (Yang and Yin 2010; Senet et al. 2013). Pan et al. (2017) derived the analytical solution of  $c_t$  and  $\varphi_t$  by analyzing plastic potential function along the rock failure surface, resulting in

$$\varphi_t = \arctan \left( \frac{A_t \sqrt{A_t + 1} + B_t C_t \left( 1/2 / \sqrt{A_t + 1} - \sqrt{A_t + 1} / (A_t + 2) \right)}{2(A_t + 1) - B_t / (A_t + 2)} \right), \tag{5}$$

$$c_t = \frac{\sigma_c C_t \sqrt{1 + A_t}}{2 + A_t} - \left( \sigma_3 + \frac{C_t}{2 + A_t} \right) \tan \varphi_t, \tag{6} \quad \mu_{\ln i} = \ln \mu_i - \frac{\sigma_{\ln i}^2}{2}. \tag{12}$$

where

$$A_t = am \left( \frac{m\sigma_3}{\sigma_c} + s \right)^{a-1}, \tag{7}$$

$$B_t = a(a - 1)m^2 \left( \frac{m\sigma_3}{\sigma_c} + s \right)^{2(a-1)}, \tag{8}$$

$$C_t = \left( \frac{m\sigma_3}{\sigma_c} + s \right)^a. \tag{9}$$

It can be seen that  $c_t$  and  $\varphi_t$  are the functions of the minimum principal stress  $\sigma_3$ . With the known Hoek–Brown parameters, the tangent line is determined by the minimum principal stress at any point inside the rock masses. It is the basis of the proposed multi-tangent method to determine the space-dependent  $c_t$  and  $\varphi_t$ . The implementation of multi-tangent method in a random field is detailed in Sect. 2.3

## 2.2 The Random Field Representation Using K-L Expansion

The fractured rock masses often show a nature of spatial variability which can be effectively modelled by the random field theory. As a TBM usually makes a minimal disturbance to the surrounding rock masses, it is only necessary to consider the spatial variability of  $m_i$ ,  $GSI$  and  $\sigma_c$ . In many practical engineering problems, the lognormally distributed random field is more advisable than the normally distributed one to represent the non-negative parameters of rock masses.  $\mu_i$ ,  $\sigma_i$ , respectively, refer to the mean value and the standard deviation of parameter  $i$ , where  $i$  can be  $m_i$ ,  $GSI$  or  $\sigma_c$ . By referring to the corresponding standard normal random field (zero mean and unit variance), the lognormal random field is given as

$$G_i(\mathbf{x}) = \exp \left[ \mu_{\ln i} + \sigma_{\ln i} G_{\ln i}(\mathbf{x}) \right], \quad i = m_i, GSI, \sigma_c, \tag{10}$$

where  $\mathbf{x}$  is a vector representing the spatial location,  $G_{\ln i}$  is the standard normal random field, and  $\mu_{\ln i}$ ,  $\sigma_{\ln i}$  can be obtained by

$$\sigma_{\ln i} = \sqrt{\ln \left( 1 + \frac{\sigma_i^2}{\mu_i^2} \right)}, \tag{11}$$

The standard normal random field is often approximately represented by a  $M$ -term K–L expansion,

$$G_{\ln i}(\mathbf{x}) \approx \sum_{j=1}^M \sqrt{\lambda_j} \xi_j \psi_j(\mathbf{x}), \tag{13}$$

where  $M$  is the number of truncation terms;  $\xi_j$  is a set of independent variables that follow the standard normal distribution;  $\lambda_j$  and  $\psi_j(\mathbf{x})$  are, respectively, the eigenvalues and the eigenfunctions of the autocorrelation function whose analytical solutions can be found in (Phoon and Ching 2014).

In practical applications, the error of Eq. (13) is inevitable, but it can be controlled within an acceptable limit by error estimation. The commonly used approach for error estimation on the K–L expansion is given as

$$\varepsilon_{err} = \frac{1}{\Omega} \int_{\Omega} \left[ 1 - \sum_{j=1}^M \lambda_j \psi_j^2(\mathbf{x}) \right] d\Omega, \tag{14}$$

where  $\Omega$  is the domain of random field. The larger the value of  $M$  is, the higher the accuracy of K–L expansion will be.

In the context of random field theory, the autocorrelation function is introduced to define the correlation between two arbitrary spatial points. In natural deposits, it can be expected that the correlation between two certain points in physical space decreases with the increase of the distance between them. This characteristic can be taken into consideration by the squared exponential autocorrelation function in a 3D random field which is given as

$$\rho_i = \exp \left\{ - \left[ \left( \frac{x_1 - x_2}{\theta_h} \right)^2 + \left( \frac{y_1 - y_2}{\theta_h} \right)^2 + \left( \frac{z_1 - z_2}{\theta_v} \right)^2 \right] \right\}, \tag{15}$$

where  $(x_1, y_1, z_1), (x_2, y_2, z_2)$ , respectively, denote the spatial coordinates of two points,  $\theta_h$  and  $\theta_v$ , respectively, denotes the horizontal and vertical autocorrelation distances. It is necessary to distinguish the horizontal and vertical autocorrelation distances since the natural deposits usually show much stronger spatial variability along vertical direction.

In addition to the autocorrelation of a random field, there probably exists the cross-correlation between two random fields which should be fully considered in the random field generations. Let  $\rho_{ij}$  denote the cross-correlation between the random fields of  $i$  and  $j$ . The lognormal random field of  $j$  can be obtained as

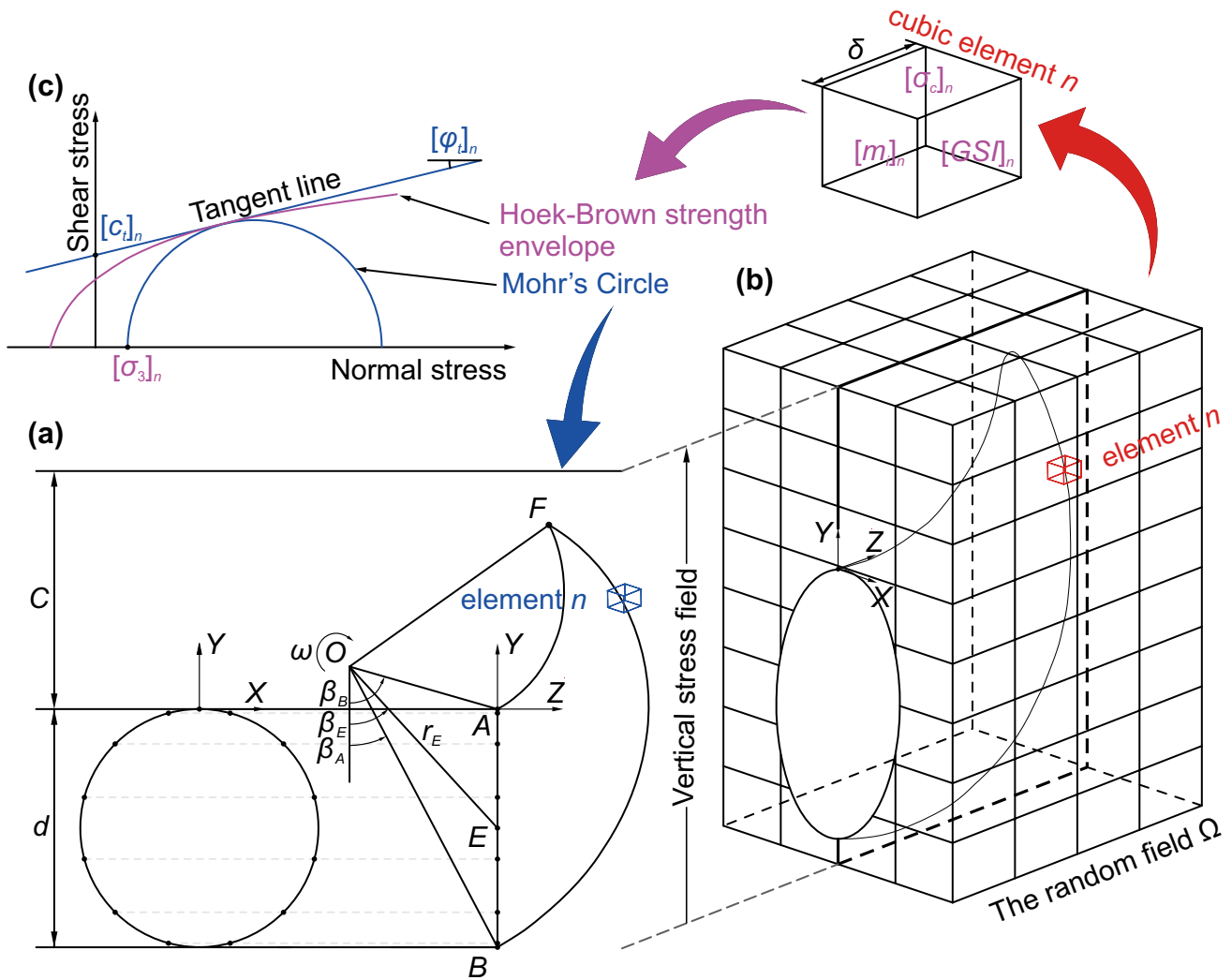


**Fig. 1** Schematic diagram for **a** 3D failure mechanism of tunnel face with a vertical stress field, **b** 3D random fields representing the spatially varying Hoek–Brown parameters  $m$ ,  $GSI$ ,  $\sigma_c$ , **c** converting the

Hoek–Brown failure criterion to Mohr–Coulomb failure criterion for element  $n$  with a multi-tangent method

$$G_j(\mathbf{x}) = \exp \left\{ \mu_{\ln j} + \sigma_{\ln j} \left[ G_{\ln i}(\mathbf{x}) \rho_{\ln i j} + G_{\ln j}(\mathbf{x}) \sqrt{1 - \rho_{\ln i j}^2} \right] \right\}, \quad j = m_i, \text{GSI}, \sigma_c, j \neq i, \tag{16}$$

where  $\rho_{\ln i j}$  is the cross-correlation coefficient between  $\ln i$  and  $\ln j$ . Fenton and Griffiths (2008) gave the relationship between  $\rho_{ij}$  and  $\rho_{\ln i j}$  as follows:

$$\rho_{\ln i j} = \frac{\ln [1 + \rho_{ij} \text{COV}(i) \text{COV}(j)]}{\sqrt{\ln [1 + \text{COV}^2(i)] \ln [1 + \text{COV}^2(j)]}}, \tag{17}$$

where  $\text{COV}(i)$  represents the coefficient of variation of random field  $i$ .

### 2.3 The 3D Rotational Failure Mechanism with Multi-tangent Method

The advanced 3D rotational failure mechanism proposed by (Mollon et al. 2011a) is adopted to characterize the face failure of a tunnel in spatially random Hoek–Brown rock masses. The 3D lognormal random field is employed to model the spatial variability of Hoek–Brown parameters,  $m_i$ , GSI and  $\sigma_c$ . As shown in Fig. 1a, a tunnel with a diameter of  $d$  and a burial depth of  $C$  is excavated in fractured Hoek–Brown rock masses. The projection of the failure mechanism on its symmetry plane is outlined by curves  $AF$  and  $BF$ , where points  $A$ ,  $B$  denote the tunnel roof and the tunnel invert, respectively.  $O$  is the rotation center and  $\omega$  is the angular velocity of the failure mechanism.  $E$  is the center point of the circular tunnel face;  $\beta_A, \beta_B, \beta_E$ , respectively, represent the inclinations of  $OA, OB$  and  $OE, r_E$  representing the length of  $OE$ . A global coordinate system  $X$ – $Y$ – $Z$  is built with its origin at the point  $A$ . For the realization of a random field, the domain  $\Omega$  that covers the possible range of tunnel face failure is discretized into rectangular elements with the side length equal to  $\delta$  in both the horizontal and vertical directions. The magnitudes of Hoek–Brown parameters at each grid point are calculated by the K–L expansion, so the magnitudes at any element can be obtained by taking the average value of its eight nodes.

In previously published works, the strength of rock masses was characterized by a single tangent line to the Hoek–Brown failure envelope (Yang and Yin 2004; Yang and Huang 2011). This can be reasonable for homogeneous rock masses, but not for spatially random rock masses. As shown in Fig. 1b, the potential failure domain ahead of tunnel face is discretized into numerous elements where the parameters  $m_i$ , GSI and  $\sigma_c$  are represented by the corresponding random fields. In order to highlight the spatially varying properties of rock masses, the tangent line to the Hoek–Brown strength envelope is defined for each element in terms of the Hoek–Brown parameters as well as the current stress state (see Fig. 1c). Equations (5) and (6) show that the tangent line is dependent on the minimum

principle stress of the element. For this purpose, the rock masses of interest are divided into several layers with equal spacing along burial depths. The minimum principle stresses of all elements in one layer is considered to be the same. The number of layers is artificially determined according to the calculation accuracy while the minimum principle stress for each layer is obtained by an optimization procedure which will be elaborated in the following. This process to calculate the equivalent shear strength parameters of spatially random rock masses in each element is called the multi-tangent method.

Incorporating with the discretization-based 3D rotational failure mechanism, the tunnel face stability can be assessed with an analytical representation. The critical face pressure of a tunnel in spatially random Hoek–Brown rock masses is formulated as

$$\sigma_T = f(m_i, \text{GSI}, \sigma_c, D | \beta_E, r_E, [\sigma_3]_n, \quad n = 1, 2, \dots, l), \tag{18}$$

where  $m_i, \text{GSI}, \sigma_c$  and  $D$  are input parameters related to the random fields; the remaining parameters are subjected to the constraints of Eq. (19) and numerically determined by an optimization procedure coded within the MATLAB platform;  $\beta_E$  and  $r_E$  are geometric parameters defining the rotational failure mechanism;  $[\sigma_3]_n$  denotes the minimum principle stress of the element  $n$  in the vertical stress field which is associated with  $c, \varphi, \gamma$  is the unit weight of rock masses;  $l$  is the number of layers in the domain  $\Omega$ ;  $h_n$  is the burial depth of the element  $n$ . More explanations about Eq. (18) are given in Appendix.

$$\begin{cases} 0 < \beta_E < \frac{\pi}{2} \\ \frac{d}{2} < r_E < 10d \\ -\sigma_c < [\sigma_3]_n < \gamma h_n \end{cases} . \tag{19}$$

## 3 Sparse Polynomial Chaos Expansion Method

### 3.1 The Polynomial Chaos Expansion

The PCE method is an effective tool to implement probabilistic analysis. It usually works as a surrogate model to predict the responses of a complex system with a significant reduction of computational time and cost (Mollon et al. 2011b; Su et al. 2018; Gong et al. 2021). Suppose

a computational model  $F$  contains  $L$  independent random variables denoted as  $\xi = [\xi_1, \xi_2, \dots, \xi_L]$ , the response  $Y$  can be represented by a PCE:

$$Y = F(\xi) \cong \sum_{j=1}^P \eta_j \psi_{\alpha}(\xi), \tag{20}$$

where  $\psi_{\alpha}(\xi)$  are the multivariate polynomials;  $\eta_j$  are the unknown coefficients of the PCE;  $P$  is the number of terms in the truncated PCE. The multivariate polynomial is equal to the product of a series of univariate polynomials  $H_{\alpha_i}(\xi_i)$ , namely

$$\psi_{\alpha}(\xi) = \prod_{i=1}^L H_{\alpha_i}(\xi_i), \tag{21}$$

where  $\alpha = [\alpha_1, \dots, \alpha_i, \dots, \alpha_L]$ ,  $\alpha_i \in \mathbb{N}$  indicating the degree of the univariate polynomial whose form depends on the distribution type of random variables (Phoon and Huang 2007; Xu and Wang 2019). For independent normal random variables, the Hermite polynomials can be used to build the analytical representation of the computational model. For correlated non-normal random variables, the Nataf transformation or Cholesky transformation can be used for de-correlation and the isoprobabilistic transformation for standard normalization. The details about the family of multivariate Hermite PC expansions can be found in (Mollon et al. 2011b).

For practical applications, a PCE must be reasonably truncated according to a certain rule in order to maintain a balance between the accuracy and the computational efficiency. A common truncation scheme suggests that only those multivariate polynomials whose total degree is not bigger than the given PCE order  $p$  are retained in Eq. (20), which can be expressed in the form of a collection as

$$A = \left\{ \alpha = [\alpha_1, \dots, \alpha_i, \dots, \alpha_L] : \sum_{i=1}^L \alpha_i \leq p \right\}. \tag{22}$$

This truncation scheme can be effective for a computational model with low-dimensional input random variables. However, for a high-dimensional problem with 100 to 200 random variables, it becomes computationally expensive. The hyperbolic truncation scheme is proposed for high-dimensional problems by defining the  $q$ -quasi-norm of  $\alpha$  as (Blatman and Sudret 2010)

$$\|\alpha\|_q = \left( \sum_{i=1}^L \alpha_i^q \right)^{\frac{1}{q}}, \quad 0 < q < 1. \tag{23}$$

The hyperbolic truncation scheme requires that the  $q$ -quasi-norm is not bigger than  $p$  which can be presented as

$$A = \left\{ \alpha = [\alpha_1, \dots, \alpha_i, \dots, \alpha_L] : \|\alpha\|_q \leq p \right\}. \tag{24}$$

The smaller the value of  $q$  is, the less the PCE terms are retained.

Then the least-square regression method can be used to determine the unknown coefficients of the PCE. Considering an experimental design (ED)  $\chi$  with a size of  $N$ ,  $\chi = [\xi^1, \dots, \xi^i, \dots, \xi^N]^T$  where  $\xi^i = [\xi_1^i, \xi_2^i, \dots, \xi_L^i]$ , the responses of the model can be obtained by running the original computational model, say the model used for determining necessary face pressures in Eq. (18), for each sample in the ED, denoted as  $Y = [Y^1, \dots, Y^i, \dots, Y^N]^T$ . According to the least-square minimization method, the PCE coefficients are obtained as

$$\hat{\eta} = (\Psi^T \Psi)^{-1} \Psi^T Y, \tag{25}$$

where  $\hat{\eta} = [\hat{\eta}_1, \hat{\eta}_2, \dots, \hat{\eta}_P]^T$  and  $\Psi$  is a space-independent matrix with dimensions of  $N \times P$  computed from the basis of the polynomials. The size  $N$  of the ED must ensure that the matrix  $\Psi^T \Psi$  is well conditioned, otherwise the ED should be enriched.

### 3.2 The PCE-Based Global Sensitivity Analysis

Even though the hyperbolic truncation scheme can effectively reduce the retained PCE terms, the computational time could still be huge when handling high-dimensional problems. The global sensitivity analysis (GSA) helps to identify the important random variables among a large number of random variables and discards the less important ones, thereby reducing the problem dimension. The Sobol’s indices are widely used in the GSA which are capable of providing the influence of one or a group of random variables on the variance of the model responses. Based on the PCE method, the analytical solution for Sobol’s index of a single random variable is expressed as

$$S(\xi_i) = \frac{\sum_{\alpha \in A_i} (\eta_j)^2 E[(\psi_{\alpha})^2]}{\sum_{\alpha \in A} (\eta_j)^2 E[(\psi_{\alpha})^2]}, \tag{26}$$

where  $\eta_j$  is the coefficient of the PCE;  $A_i$  is a subset of  $A$  defined by

$$A_i = \left\{ \alpha = [\alpha_1, \dots, \alpha_i, \dots, \alpha_L] : \alpha_i > 0, \alpha_k = 0, k \in [1, L], k \neq i \right\}, \tag{27}$$

and

$$E[(\psi_{\alpha})^2] = \prod_{i=1, \alpha_i \in A} \alpha_i! \tag{28}$$

Since the PCE order has little influence on the Sobol's indices, it is possible to reduce the problem dimension by finding the important variables with a low-order PCE, such as second or third order, and then building a high-order PCE with the reduced dimension (Al-Bittar and Soubra 2014). An effective scheme to discard the less important random variables was proposed by (Al-Bittar and Soubra 2014). The value of 2% of the Sobol's index of the first important random variable is regarded as a threshold. Only random variables with Sobol's indices bigger than this threshold are kept to build the high order PCE. Other random variables that cannot reach this threshold are considered as deterministic parameters and replaced by their mean values.

### 3.3 The Adaptive Sparse PCE Method

To further improve computational efficiency of the PCE, a sparsity scheme was proposed by (Blatman and Sudret 2010) to approximate the computational model with a small number of significant basis functions in the PCE. This is called as a SPCE. In this paper, an adaptive regression-based algorithm is used to automatically detect the significance of each term for building a SPCE and the leave-one-out cross-validation is employed to check the accuracy of a SPCE model. This algorithm roughly consists of the following two steps: the forward step and the subsequent backward step. The forward step aims to select the significant candidate terms from the PCE basis determined by Eq. (24). In this step, the coefficient of determination  $R^2$  is considered as an indicator, by which a term leading to a significant increase of  $R^2$ , greater than  $\varepsilon_{\text{cut}}$ , can be retained. In the backward step, the less important terms in the retained PCE basis, namely those leading an insignificant reduction of  $R^2$ , smaller than  $\varepsilon_{\text{cut}}$ , are discarded. These two steps are alternately performed

until either the target accuracy  $Q_{\text{tgt}}^2$ , or the maximum PCE order  $p_{\text{max}}$  is reached. The details about the stepwise regression algorithm and the SPCE are available in (Blatman and Sudret 2010).

## 4 Probabilistic Model for a Rock Tunnel Face with Spatial Variability

### 4.1 Statistics of Hoek–Brown Parameters for Fractured Rock Masses

The latest version of Hoek–Brown failure criterion is able to characterize the tunnel face failure varying from the intact rock to the heavily fractured rock masses. To give reasonable ranges of the Hoek–Brown parameters in low-quality rock masses, the researchers have made a large number of statistically based estimations of Hoek–Brown parameters (Hoek et al. 2002; Sari et al. 2010; Li et al. 2012; Senent et al. 2013). It is reported that in heavily fractured rock masses, the mean value of  $m_i$  ranges from 4 to 15, GSI from 10 to 30 and  $\sigma_c$  from 1 to 30 MPa. Due to the inherent uncertainties in nature rock deposits, the coefficients of variations (COVs) of Hoek–Brown parameters are of great importance for tunnel face stability assessment. In addition, studies considering the spatial variability of rock masses should emphasize the values of autocorrelation distances which are crucial parameters in building a random field.

Table 1 summarizes the commonly used statistical properties of Hoek–Brown parameters as well as the corresponding research methods and topics in previously published works. Totally speaking,  $\text{COV}(m_i)$  is bounded between 10 and 20% while  $\text{COV}(\text{GSI})$  ranges from 3 to 25%.  $\text{COV}(\sigma_c)$

**Table 1** A summary of COVs and spatial variability of Hoek–Brown parameters in previous studies

Refs	Method	Topic	COV/%				Autocorrelation distance/m	
			$m_i$	GSI	$\sigma_c$	$D$	$\theta_h$	$\theta_v$
Al-Bittar and Soubra (2017)	Probabilistic analysis; SPCE; Random field	Bearing capacity of a strip footing	0	5–10	12.5–37.5	0	0.5–100	0.5–100
Lü and Low (2011)	Probabilistic analysis; Response surface method; Second-order reliability method	Tunnel convergence of rock excavations	13	10	25	0	–	–
Sari et al. (2010)	Stochastic modeling technique; Monte Carlo simulation	Rock mass properties estimation	15.4–24.6	7.7–15.3	74.7–44.3	0	–	–
Pan and Dias (2018)	Probabilistic analysis; Limit analysis; PCE	Tunnel face stability in rock masses	11	18	22	15	–	–
Li et al. (2012)	Probabilistic analysis; Monte Carlo simulation; Limit analysis	Rock slope failure	12.50	3.3–5.6	25	0	–	–
Lü et al. (2018)	Probabilistic analysis; Response surface method; Random field	Rock tunnel convergence	17	8	37.50	0	4–40	4–40
Song et al. (2011)	Deterministic analysis; FLAC3D simulation; Random field	Rock tunnel behaviors	–	6–25	18–43	0	0.1–10	0.1–0



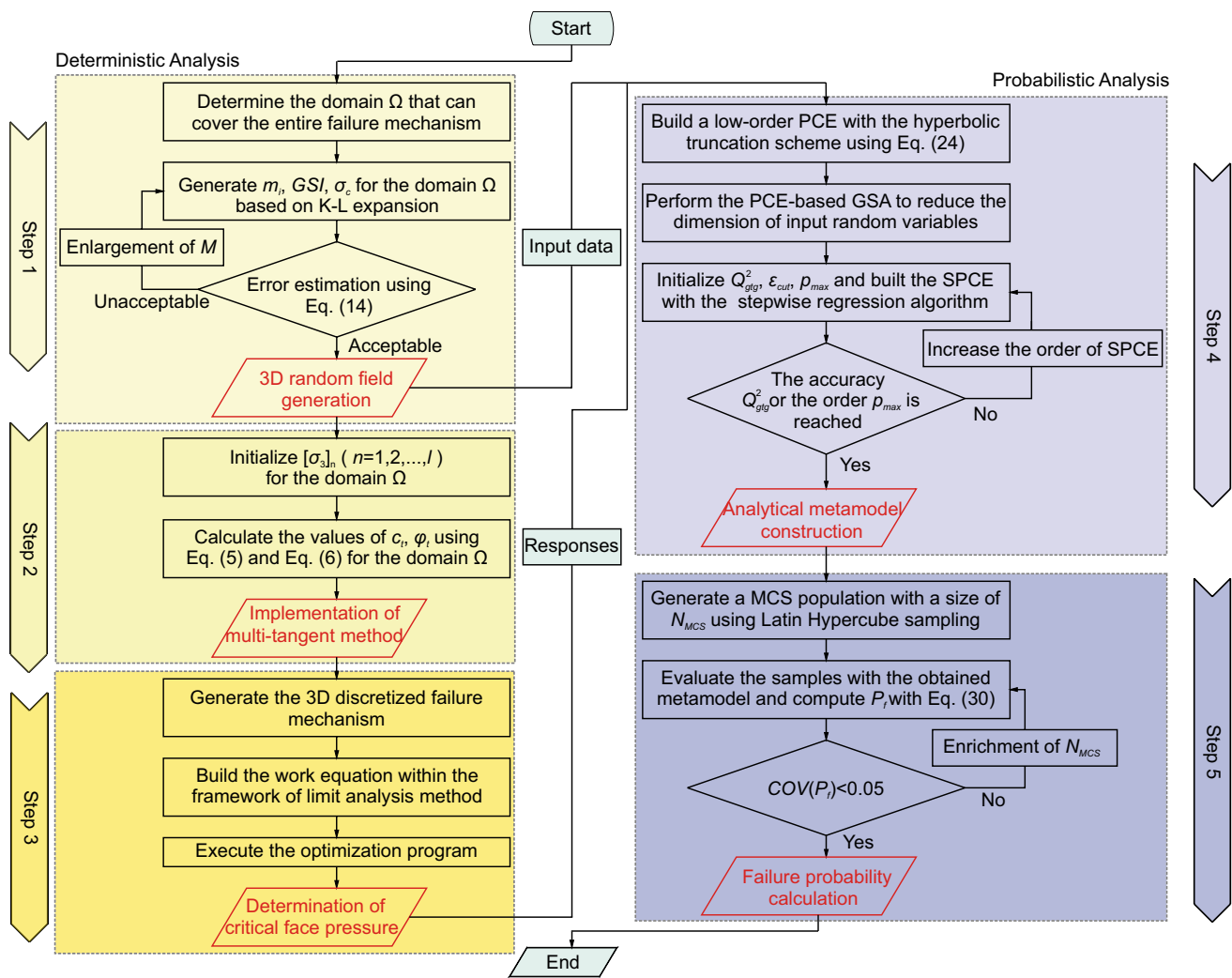


Fig. 2 Flow chart of the proposed probabilistic model

has a relatively wide range from 10 to 40%. (Sari et al. 2010) presented a COV( $\sigma_c$ ) as big as 74.7% which came from the statistical analyses of Ankara andesites at three distinct weathering grades.  $D$  often takes 0 for underground excavations representing a minimal disturbance to surrounding rocks, such as a shield-driven excavation.

### 4.2 Probabilistic Stability Analysis

Based on the above analysis, an analytical metamodel can be constructed with the SPCE method for the representation of tunnel face failure in spatially random Hoek–Brown rock masses. In combination of Monte Carlo simulation (MCS), this method can give the probabilistic density function (PDF) of critical face pressure with only a few calls to the original computational model. It is assumed that a uniform pressure  $\sigma_U$  is applied on the tunnel face, so the performance function can be given as

Table 2 Statistical properties of input variables

Random variable	Mean value	COV (%)	Distribution type	Cross-correlation coefficient
$m_i$	5	11	Lognormal	$\rho_{m_i, GSI} = -0.25$
$GSI$	15	18	Lognormal	$\rho_{GSI, \sigma_c} = 0.3$
$\sigma_c$	1 MPa	22	Lognormal	$\rho_{m_i, \sigma_c} = -0.4$
$\sigma_U$	–	15	Lognormal	–

$$g_T = \sigma_U - \sigma_T, \tag{29}$$

where  $\sigma_T$  is the critical face pressure computed by Eq. (18) or by the obtained metamodel.  $g_T \geq 0$  indicates a stable tunnel face while  $g_T < 0$  corresponds to an unstable tunnel face. In this paper,  $\sigma_U$  is modelled as a random variable that follows the lognormal distribution with the COV equal to 15%.

The failure probability of tunnel face  $P_f$  can be obtained by a metamodel-based MCS as follows.

$$P_f = \frac{1}{N_{MCS}} \sum_{i=1}^{N_{MCS}} I[g_T(i)], \tag{30}$$

where  $N_{MCS}$  denotes the size of MCS population;  $i$  refers to the  $i$ -th individual in the MCS population;  $I(x)$  is an indicator function with  $I(x) = 1$  for  $x < 0$  and  $I(x) = 0$  for  $x \geq 0$ . The COV of  $P_f$  can be computed by

$$COV(P_f) = \sqrt{\frac{1 - P_f}{N_{MCS} P_f}}, \tag{31}$$

where  $COV(P_f) < 0.05$  means a reliable result for practical applications.

Figure 2 presents the detailed process to perform the probabilistic stability analysis of tunnel face in spatially random Hoek–Brown rock masses with a multi-tangent method. It consists of five steps with a progressive relationship between them. The first three steps focus on a deterministic computational model of tunnel face failure using the kinematical approach of limit analysis and the last two steps aim to compute the failure probability of tunnel face by combining SPCE method with MCS.

1. 3D random field generation. The 3D random fields are generated using K–L expansion to model the spatial varying Hoek–Brown parameters of rock masses ahead of tunnel face. Based on the literature given in Table 1, the basic parameter settings for input variables in this paper are provided in Table 2. The lognormal distribution is used to exclude the negative values of variables that may be generated in stochastic sampling. The diameter of tunnel face  $d$  is taken as 10 m. The domain of random field is bounded in the range of  $\Omega$ :  $-5 \text{ m} < X < 5 \text{ m}$ ,  $-10 \text{ m} < Y < 10 \text{ m}$ ,  $0 < Z < 10 \text{ m}$ , which can guarantee that the failure mechanism does not exceed this range. The element size  $\delta$  is set to 0.5 m which is fine enough for good results. The unit weight of rock masses  $\gamma$  is set to  $25 \text{ kg/m}^3$ . Shokri et al. (2019) gave the reference values of the autocorrelation distances  $\theta_h, \theta_v$  by collecting data from different published papers. Based their recommendations, this paper considers the autocorrelation distances of  $\theta_h = 10 \text{ m}, 20 \text{ m}, 30 \text{ m}, 40 \text{ m}$  and  $\theta_v = 4 \text{ m}, 6 \text{ m}, 8 \text{ m}, 10 \text{ m}$ . Three lognormal random fields, respectively corresponding to  $m_i, GSI$  and  $\sigma_c$ , are generated based on the K–L expansion. One realization of the three random fields will assign values of  $m_i, GSI$  and  $\sigma_c$  to each grid point of the elements which constitutes the basis of subsequent calculations.
2. Implementation of multi-tangent method. As mentioned above, the single tangent line to represent the rock

strength of the whole failure mechanism is not effective any more for spatially random rock masses. To take into account this issue, a series of tangent lines are employed to determine the equivalent shear strength parameters  $c_i$  and  $\phi_i$  for each element in the random fields. In each element, the Hoek–Brown parameters can be calculated by averaging the values of  $m_i, GSI$  or  $\sigma_c$  at the eight grid points of the element. With the initialized value of minimum principle stress  $\sigma_3$  of each element, the equivalent shear strength parameters can be obtained by Eqs. (5) and (6). Here the value of  $\sigma_3$  is a parameter dependent on an optimization procedure. To avoid excessive computing burden, the rock masses are divided into several layers with equal spacing of  $h_{st}$  along the depth and  $\sigma_3$  takes the same value for one layer. In this paper,  $h_{st}$  is set to 1 m. As a consequence, there are 20 parameters, namely  $[\sigma_3]_n$  ( $n = 1, 2, \dots, 20$ ), to be optimized for the rock masses from  $Y = -10 \text{ m}$  to  $Y = 10 \text{ m}$ . The optimization procedure will be introduced in the next step.

3. Determination of critical face pressure. With the determined Hoek–Brown parameters at each element, the equivalent shear strength parameters of rock masses can be calculated. Then the 3D rotational failure mechanism of tunnel face is generated point by point. Details about this process can be found in (Mollon et al. 2011a). An optimization procedure coded within the framework of *MATLAB* platform is used to search the critical face pressures with the object function of Eq. (18) where the value of  $l$  is 20. It is noted that there are 22 optimization variables in total which seems to be intractable for the traditional optimization scheme. In this study, the Genetic Algorithm (GA) is combined with the Sequence

**Table 3** Values of  $M$  for cases with different autocorrelation distances

No	$\theta_h/\text{m}$	$\theta_v/\text{m}$	$\epsilon_{err}$ in Eq. (14)	$M$
1	10	4	$9.90 \times 10^{-2}$	225
2	10	6	$9.85 \times 10^{-2}$	175
3	10	8	$9.87 \times 10^{-2}$	135
4	10	10	$9.96 \times 10^{-2}$	110
5	20	4	$9.97 \times 10^{-2}$	95
6	20	6	$9.91 \times 10^{-2}$	65
7	20	8	$9.95 \times 10^{-2}$	50
8	20	10	$9.47 \times 10^{-2}$	45
9	30	4	$9.68 \times 10^{-2}$	60
10	30	6	$9.81 \times 10^{-2}$	40
11	30	8	$9.94 \times 10^{-2}$	30
12	30	10	$9.90 \times 10^{-2}$	25
13	40	4	$9.59 \times 10^{-2}$	50
14	40	6	$9.38 \times 10^{-2}$	35
15	40	8	$9.85 \times 10^{-2}$	25
16	40	10	$8.77 \times 10^{-2}$	25

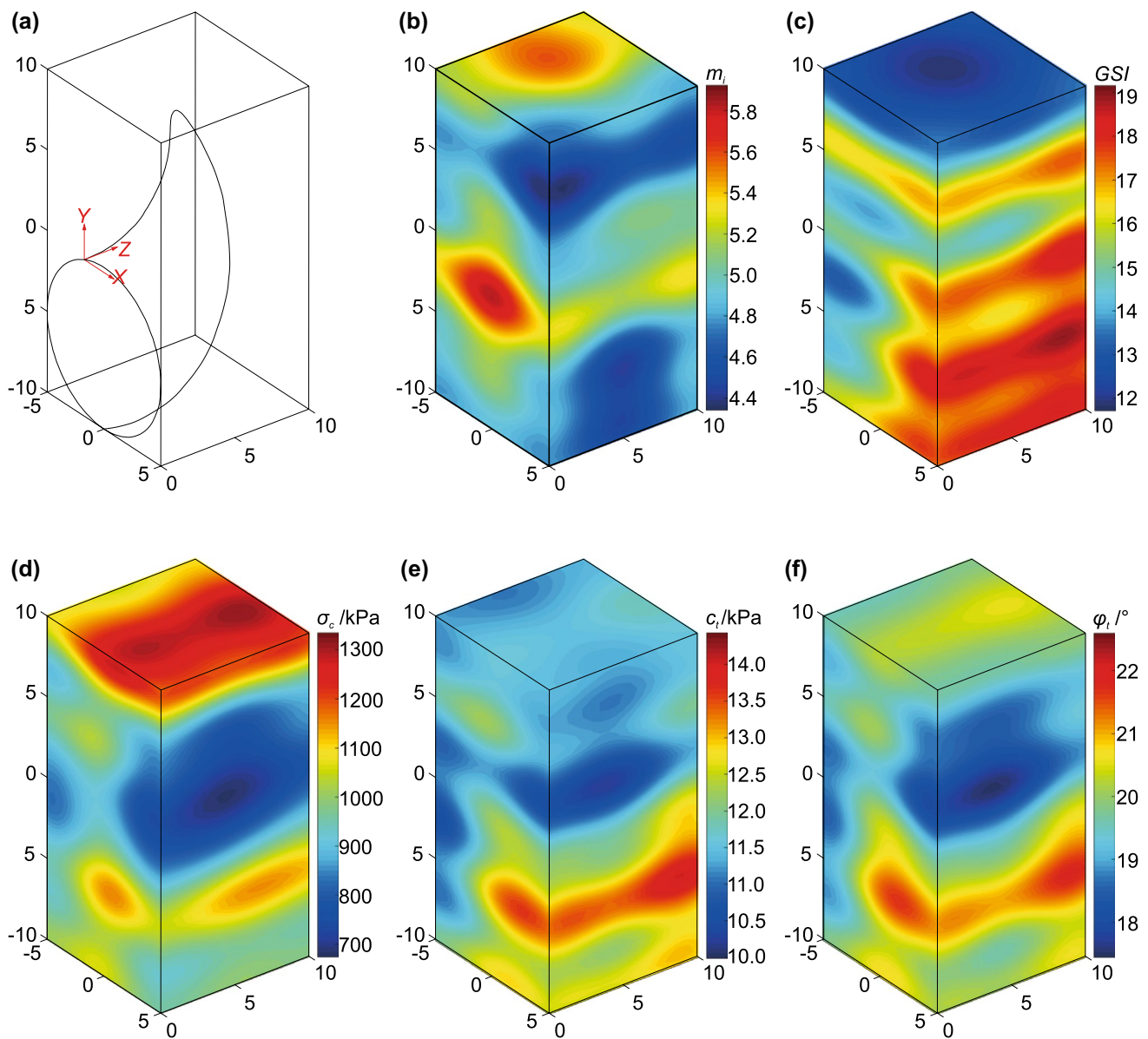


**Fig. 3** Illustration for **a** tunnel face failure, one realization of random fields of, **b**  $m_i$ , **c** GSI, **d**  $\sigma_c$ , and the computed random fields of, **e**  $c_i$ , **f**  $\phi_i$

Quadratic Programming (SQP) to search for the optimal set of parameters which maximize Eq. (18).

- Analytical metamodel construction. Once the random fields of Hoek–Brown parameters and the corresponding model responses are determined, they can be used to build the SPCE metamodel. This process has been elaborated in Sect. 3. The SPCE that satisfies the stopping criterion is taken as an analytical metamodel for evaluating the failure probability of tunnel face. In this step, the involved parameters for the SPCE construction

are initialized as: the target accuracy  $Q_{gtg}^2$  of 0.999, the cutoff value  $\epsilon_{cut}$  of  $5 \times 10^{-5}$ , the maximal order  $p_{max}$  of 5 and  $q=0.7$ .

- Failure probability calculation. This step is a traditional MCS process by replacing the original deterministic model with the obtained analytical metamodel. The Latin Hypercube Sampling is used to generate the MCS samples as evenly as possible in the sampling space. The failure probability of tunnel face is calculated with Eq. (30). The result that satisfies  $COV(P_f) < 0.05$  is accepted as the final failure probability.

**Table 4** Comparison with the results given by (Senent et al. 2013)

Case	Rock parameters				Critical face pressure/kPa			Difference between two limit analysis method (%)
	$m_i$	GSI	$\sigma_c$ /MPa	$\gamma$ /kN·m <sup>-3</sup>	FLAC3D from (Senent et al. 2013)	Limit analysis by (Senent et al. 2013)	Presented limit analysis solution	
1	5	10	1	25	61.9	52.0	56.5	7.96
2	5	15	1	25	38.6	36.8	39.19	6.10
3	5	20	1	25	26.3	26.8	29.36	8.72
4	5	25	1	25	18.9	20.3	22.03	7.85
5	5	10	5	25	15.3	17.1	18.78	8.95
6	5	15	5	25	8.30	9.80	10.26	4.48
7	5	20	5	25	5.30	5.20	5.29	1.70
8	5	25	5	25	2.40	2.30	2.47	6.88
9	10	10	1	25	26.4	27.6	29.97	7.91
10	15	10	1	25	17.1	18.9	20.69	8.65

## 5 Results and Discussions

### 5.1 Determination of $M$ in the K–L Expansion

The number of retained terms in a K–L expansion  $M$  should be determined prior to the random field generation. It can be achieved by checking the error produced by the truncated K–L expansion iteratively until the error is less than a prescribed one. In this paper, the prescribed error is set to 10%. The error estimation is performed using Eq. (14) which should be satisfied to determine the value of  $M$ . The results

are given in Table 3 where  $\theta_h$  ranges from 10 to 40 m and  $\theta_v$  from 4 to 10 m. It can be seen that less terms are retained in the K–L expansion with a bigger autocorrelation distance.

### 5.2 Discussions on the Deterministic Computational Model

The deterministic computational model of tunnel face failure is analytically expressed as an implicit function of Eq. (18), which is involved with the random fields, the multi-tangent method and the kinematically admissible velocity field.

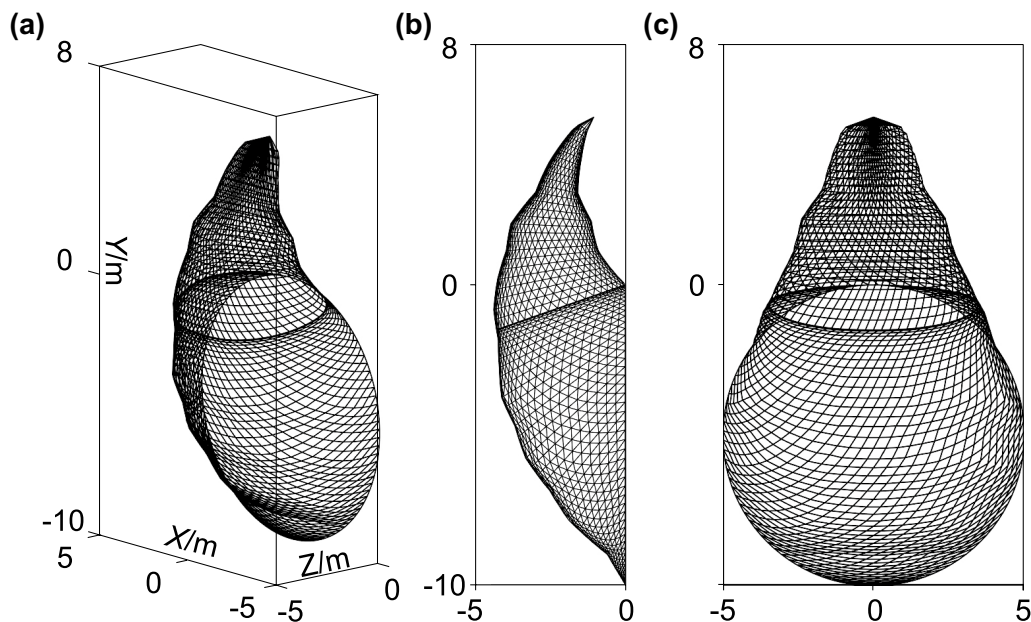


**Fig. 4** Views of the critical failure mechanisms of Case 1 in Table 4 **a** 3D view, **b** side view, **c** front view

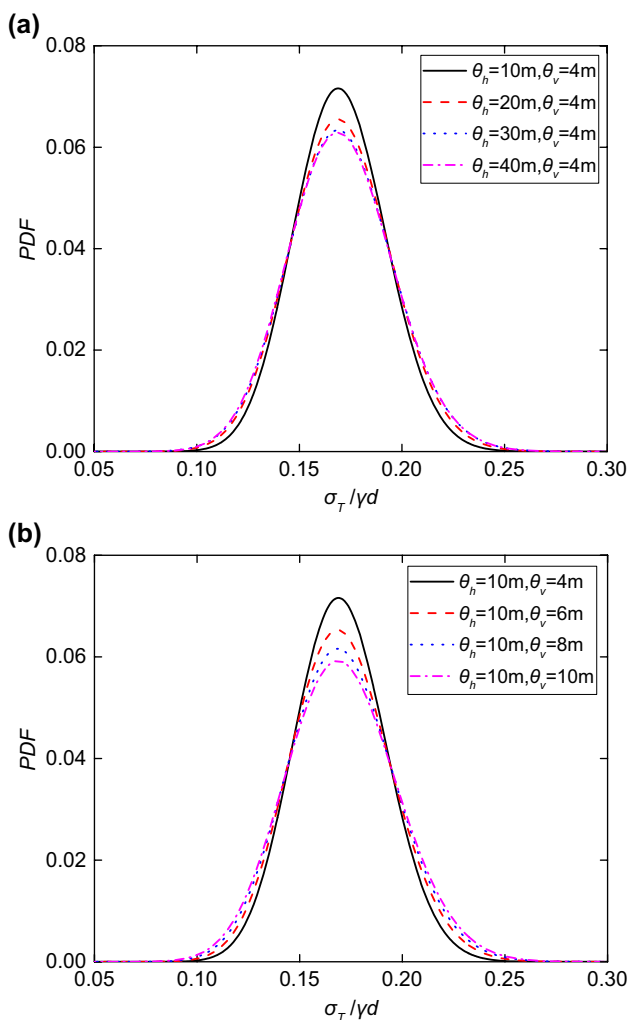


**Fig. 5** PDFs of normalized critical face pressure with different **a** horizontal autocorrelation distances, and **b** vertical autocorrelation distances

Figure 3a illustrates the tunnel face excavation in spatially random Hoek–Brown rock masses. Figure 3b–d shows one realization of random field generations, respectively, for  $m_i$ , GSI, and  $\sigma_c$  with their statistical properties in Table 2 and the autocorrelation distances of  $\theta_h = 10$  m,  $\theta_v = 4$  m. In this model, the total number of parameters that need to be optimized is up to 22, including 2 parameters determining the geometrical pattern of the failure mechanism and 20 parameters involved with the equivalent shear strength parameters of rock masses in the domain  $\Omega$ . By performing the above-mentioned optimization program, the final result can be obtained with the corresponding random fields of  $c_t$  and  $\varphi_t$  as shown in Fig. 3e, f.

In order to validate the proposed deterministic model, the cases studied in (Senent et al. 2013) are revisited here. This literature did not consider the spatial variability of Hoek–Brown rock masses, but assumed a linear

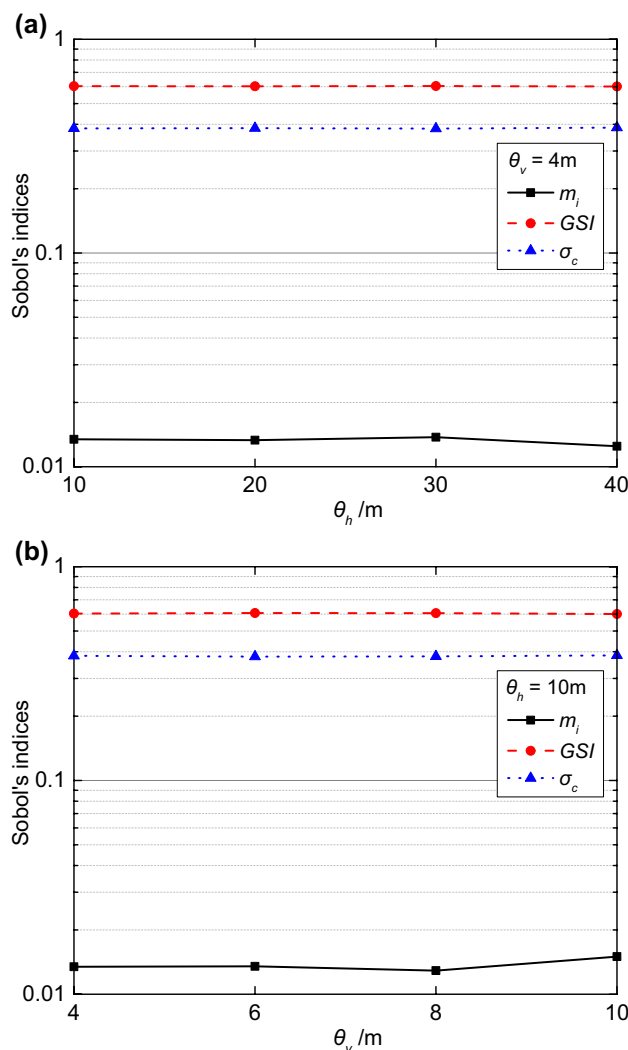


**Fig. 6** Sobol's indices of  $m_i$ , GSI and  $\sigma_c$  versus **a** horizontal autocorrelation distances, and **b** vertical autocorrelation distances

stress distribution with depth. In each case, the values of Hoek–Brown parameters in (Senent et al. 2013) are used to replace the mean values in Table 2. The COVs are set to 0 which indicates a uniform rock mass without spatial variability. These settings guarantee the same input data with the study of (Senent et al. 2013). A further comparison with the finite difference method of FLAC3D has been performed in (Senent et al. 2013) which will be referred to but not to reproduced. The comparison results are summarized in Table 4. It can be observed that the critical face pressures estimated by the presented approach are bigger than the ones given by (Senent et al. 2013) in all cases. The results are relatively in good agreement with each other despite the biggest difference of 8.95%. This is partly because the equivalent shear strength parameters are derived from the plastic potential function analysis in the presented research (see Eqs. (5) and (6)), and partly due to the vertical stress

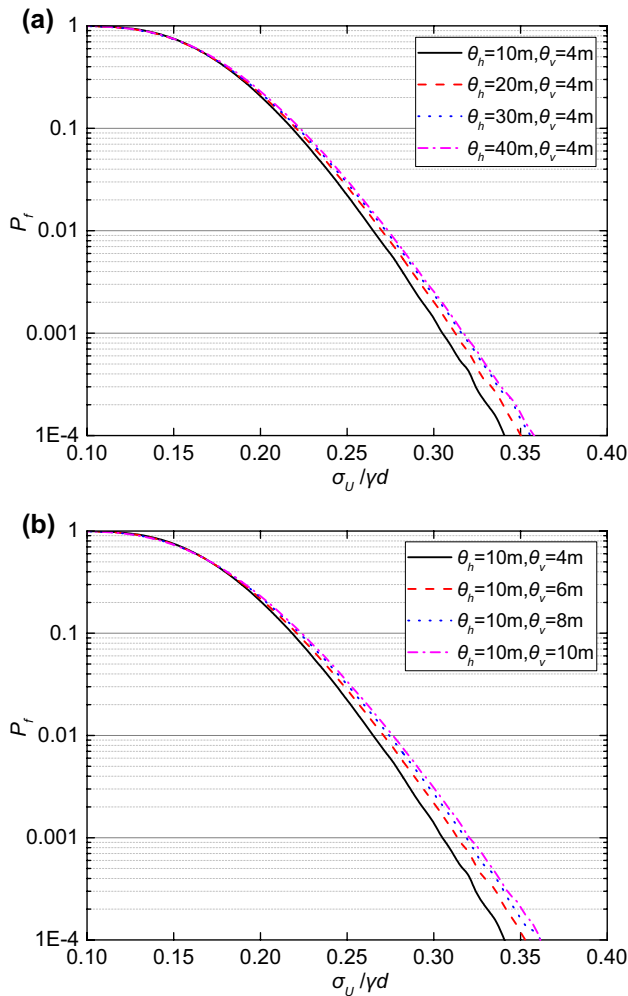


**Fig. 7** Failure probability of tunnel face versus the normalized applied face pressures with different **a** horizontal autocorrelation distances, and **b** vertical autocorrelation distances

field optimization rather than a predefined stress distribution in (Senent et al. 2013). Figure 4 presents the views of the failure mechanism of Case 1 in Table 4 provided by the presented approach. It is of interest to see that the failure surface is not as smooth as the one plotted by (Senent et al. 2013). This is attributed to the spatial variability of rock masses considered in this study.

### 5.3 The Probability Density Functions of Critical Face Pressures

Figure 5 shows the PDFs of the normalized critical face pressure  $\sigma_T/\gamma d$  with different autocorrelation distances. The statistical properties of input variables listed in Table 2 are used for the following studies. By comparing Fig. 5a, b, we can know that the variation of vertical autocorrelation distance has a stronger influence on the PDF curves than that of the horizontal one. Both the two plots show that the

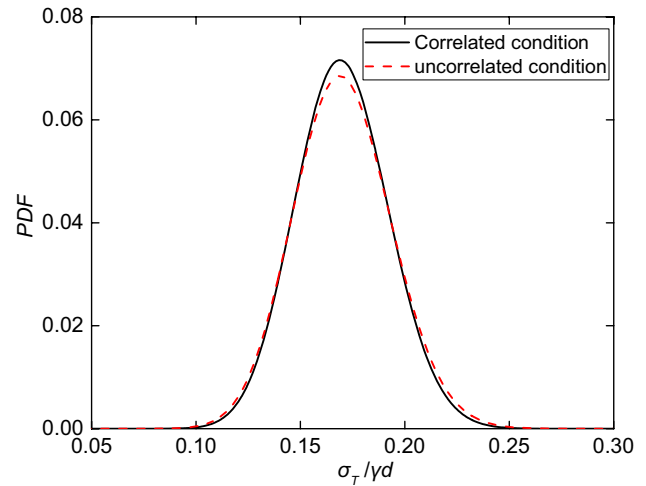


**Fig. 8** The influence of cross-correlations of random fields on PDF curves of normalized critical face pressure

increase of autocorrelation distances leads to a lower but wider PDF curve of the normalized critical face pressure. In other words, the decrease of autocorrelation distances results in a more concentrated distribution of critical face pressures which indicates a smaller required face pressure for a target failure probability.

Figure 6 presents the Sobol’s indices of  $m_i$ , GSI and  $\sigma_c$  with the autocorrelation distances corresponding to the cases in Fig. 5. According to the Sobol’s indices, the most important Hoek–Brown parameter influencing tunnel face stability is the GSI, which is followed by  $\sigma_c$  and  $m_i$ . Besides, it is interesting to see that the autocorrelation distance has a limited influence on the Sobol’s indices. As we known, the random field gradually approaches a random variable as the autocorrelation distance increases. This implies that

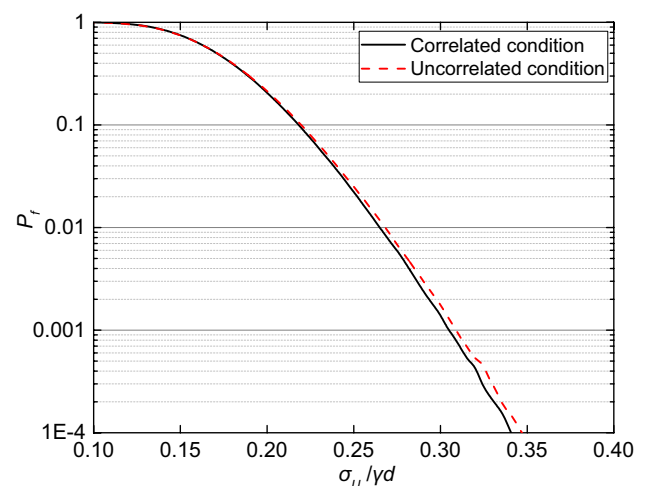


**Fig. 9** The influence of cross-correlations of random fields on tunnel face failure probabilities

taking soil parameters as random fields or random variables has no significant difference in sensitivity analysis of input parameters.

#### 5.4 The Failure Probability of Tunnel Face

By giving a series of mean values of applied face pressure  $\sigma_U$ , the failure probabilities of tunnel face are calculated and plotted in Fig. 7.  $\sigma_U$  is considered as a lognormally distributed random variable with  $\text{COV}(\sigma_U) = 15\%$  and normalized by  $\gamma d$ . It is not surprising that the failure probability decreases with the increase of  $\sigma_U$ . By referring to this figure, one can find out the necessary face pressure corresponding to a target failure probability. The increase of autocorrelation distance generates a bigger failure probability of tunnel face, which is consistent with the conclusions from Fig. 5. Thus it can be speculated that ignoring the spatial variability of rock properties leads to a conservative result in the engineering design. It is of interest to find a similar observation with Fig. 5 that the vertical autocorrelation distance has a more obvious effect on the failure probability than the horizontal one.

#### 5.5 The Influence of Cross-Correlations of Random Variables

An extensive database of rock triaxial tests shows that  $m_i$ ,  $GSI$  and  $\sigma_c$  are correlated rather than completely independent (Zeng et al. 2016; Shen and Karakus 2014). Zeng et al. (2016) proposed a correlation relationship among these parameters by analyzing several data groups of  $m_i$ ,  $GSI$  and  $\sigma_c$  for different rock types. The cross-correlation coefficients of the input variables are given in Table 2. This section is devoted to the influence of cross-correlations of Hoek–Brown parameters on the PDF curves and the failure probability of tunnel face. Figure 8 presents the PDF curves of normalized critical face pressures, respectively, corresponding to the correlated and uncorrelated conditions with  $\theta_h = 10$  m and  $\theta_v = 4$  m. The correlated condition take into consideration the cross-correlations among the random fields of  $m_i$ ,  $GSI$  and  $\sigma_c$  while the uncorrelated condition does not consider the cross-correlations. It is observed that ignoring the cross-correlations leads to a more spread-out distribution which suggests a bigger variability of the critical face pressures. Figure 9 gives the failure probability of tunnel face versus normalized applied face pressure. It can be seen that the uncorrelated condition requires a bigger face pressure than the correlated one for a target failure probability. So it can be inferred that ignoring the cross-correlations of  $m_i$ ,  $GSI$  and  $\sigma_c$  can result in a conservative design for practical engineering.

## 6 Conclusion

This paper presents an efficient approach for probabilistic stability analysis of tunnel face driven in heavily fractured rock masses that follow Hoek–Brown failure criterion. The random field theory is used to model the spatial variabilities of  $m_i$ ,  $GSI$  and  $\sigma_c$ . The multi-tangent line method allows the rock masses at different locations to have different equivalent shear strength parameters according to their Hoek–Brown parameters and the stress state. The discretized rotational failure mechanism is used to estimate the critical face pressure of a rock tunnel. The SPCE method is combined with GSA for establishment of the analytical metamodel with a reduced dimension of input variables. The following conclusions can be drawn:

The deterministic computational model is compared with that proposed by (Senent et al. 2013) which shows that the presented solutions are bigger than those given by (Senent et al. 2013). The maximum difference in the 10 selected cases is 8.95%. It is partly because the equivalent shear strength parameters are derived from the plastic potential function analysis in the presented research (see Eqs. (5) and (6)) and partly due to the vertical stress field optimization rather than a predefined stress distribution in (Senent et al. 2013).

The PDF curves of critical face pressure and the failure probability of tunnel face are affected by the spatial variabilities of  $m_i$ ,  $GSI$  and  $\sigma_c$ . Results show that the decrease of autocorrelation distance results in a big peak value of the PDF curve, which indicates a concentrated distribution of critical face pressure. It can be speculated that ignoring the spatial variabilities of rock properties (infinite autocorrelation distances) leads to a conservative result in the engineering design.

Studies on the influence of cross-correlation of random variables show that ignoring the cross-correlations leads to a less concentrated distribution of critical face pressure which can produce a conservative design for practical engineering.

### Appendix: Work rate equation for face stability analysis

Let  $\sigma_T$  denotes the pressure provided by the shield machine to retain tunnel face stability, so its work rate can be calculated by

$$W_{\sigma_T} = \iint_S \vec{\sigma}_T \cdot \vec{v} dS = -\omega \sigma_T \sum_j (S_{j0} R_{j0} \cos \beta_{j0}), \quad (32)$$

where  $S_{j0}$  is the area of the  $j$ -th element on tunnel face;  $R_{j0}$  is the corresponding rotation radius;  $\beta_{j0}$  is the angle between the rotation radius and the negative direction of the  $Y$ -axis.

The work rate done by gravity of rock masses can be calculated as

$$W_\gamma = \iiint_V \vec{\gamma} \cdot \vec{v} dV = \omega \gamma \sum_i \sum_j (V_{ij} R_{ij} \sin \beta_{ij}), \quad (33)$$

where  $\gamma$  is the unit weight of rock masses;  $V_{ij}$  is the volume of the element determined by local coordinate system;  $R_{ij}$  is the corresponding rotation radius;  $\beta_{ij}$  is the angle between the rotation radius and the negative direction of the  $Y$ -axis.

The internal energy dissipation can be expressed by

$$W_D = \sum \iint_S c_t \cdot v \cdot \cos \varphi_t dS = \omega \sum_i \sum_j ([c_t]_{ij} \cos [\varphi_t]_{ij} S_{ij} R_{ij}), \quad (34)$$

where  $[c_t]_{ij}$  and  $[\varphi_t]_{ij}$  represent the corresponding equivalent cohesion and internal friction angle of the element;  $S_{ij}$  denotes the elementary area on the failure surface and  $R_{ij}$  is the corresponding rotation radius.

By equating the internal energy dissipation and external work rate, the required face pressure can be obtained as

$$\sigma_T = \gamma d N_\gamma - N_c, \quad (35)$$

where  $N_\gamma$ ,  $N_c$  are non-dimensional coefficients as

$$N_\gamma = \frac{\sum_i \sum_j (V_{ij} R_{ij} \sin \beta_{ij})}{d \sum_j (S_{j0} R_{j0} \cos \beta_{j0})}, \quad (36)$$

$$N_c = \frac{\sum_i \sum_j ([c_t]_{ij} \cos [\varphi_t]_{ij} S_{ij} R_{ij})}{\sum_j (S_{j0} R_{j0} \cos \beta_{j0})}. \quad (37)$$

The expressions of  $[c_t]_{ij}$  and  $[\varphi_t]_{ij}$  are specified by Eqs. (5) and (6). They are determined by the Hoek–Brown parameters and the stress state of the element of interest. More details for the derivation can be obtained from (Mollon et al. 2011a).

**Acknowledgements** This study was financially supported by National Natural Science Foundation of China (Grant No. 42102321 and Grant No. 52108388), The National Key Research and Development Program of China (Grant No. 2017YFE0119500) and the Fundamental Research Funds for the Central Universities, China University of Geosciences (Wuhan) (Grant No. CUGGC09). The financial funding is greatly appreciated.

## References

Al-Bittar T, Soubra AH (2014) Efficient sparse polynomial chaos expansion methodology for the probabilistic analysis of

- computationally-expensive deterministic models. *Int J Numer Anal Meth Geomech* 38(12):1211–1230
- Al-Bittar T, Soubra AH (2017) Bearing capacity of spatially random rock masses obeying Hoek–Brown failure criterion. *Georisk Assess Manag Risk Eng Syst Geohazards* 11(2):215–229
- Blatman G, Sudret B (2010) An adaptive algorithm to build up sparse polynomial chaos expansions for stochastic finite element analysis. *Probab Eng Mech* 25(2):183–197
- Blatman G, Sudret B (2011) Adaptive sparse polynomial chaos expansion based on least angle regression. *J Comput Phys* 230(6):2345–2367
- Chen F, Wang L, Zhang W (2019) Reliability assessment on stability of tunnelling perpendicularly beneath an existing tunnel considering spatial variabilities of rock mass properties. *Tunn Undergr Space Technol* 88:276–289
- Dadashzadeh N, Duzgun HSB, Yesiloglu-Gultekin N (2017) Reliability-based stability analysis of rock slopes using numerical analysis and response surface method. *Rock Mech Rock Eng* 50(8):2119–2133
- Fenton GA, Griffiths DV (2003) Bearing-capacity prediction of spatially random  $c \phi$  soils. *Can Geotech J* 40(1):54–65
- Fenton GA, Griffiths DV (2008) Risk assessment in geotechnical engineering. Wiley, Hoboken
- Gong W, Juang CH, Wasowski J (2021) Geohazards and human settlements: lessons learned from multiple relocation events in Badong China—Engineering geologist’s perspective. *Eng Geol* 285:106051
- Guo X, Du D, Dias D (2019) Reliability analysis of tunnel lining considering soil spatial variability. *Eng Struct* 196:109332
- Hoek E, Brown ET (1997) Practical estimates of rock mass strength. *Int J Rock Mech Min Sci* 34(8):1165–1186
- Hoek E, Carranza-Torres C, Corkum B (2002) Hoek–Brown failure criterion—2002 edition. *Proc NARMS-Tac* 1(1):267–273
- Hoek E, Brown ET (1980) Empirical strength criterion for rock masses. *J Geotech Geoenviron Eng* 106(ASCE 15715)
- Huang F, Wang D, Xiao N, Ou RC (2021) Upper bound limit analysis of blow-out failure mode of excavation face of shield tunnel considering groundwater seepage. *Geomech Eng* 26(3):227–234
- Jiang SH, Li DQ, Cao ZJ, Zhou CB, Phoon KK (2015) Efficient system reliability analysis of slope stability in spatially variable soils using Monte Carlo simulation. *J Geotech Geoenviron Eng* 141(2):04014096
- Leca E, Dormieux L (1990) Upper and lower bound solutions for the face stability of shallow circular tunnels in frictional material. *Geotechnique* 40(4):581–606
- Li AJ, Cassidy MJ, Wang Y, Merifield RS, Lyamin AV (2012) Parametric Monte Carlo studies of rock slopes based on the Hoek–Brown failure criterion. *Comput Geotech* 45:11–18
- Li T, Gong W, Tang H (2021) Three-dimensional stochastic geological modeling for probabilistic stability analysis of a circular tunnel face. *Tunn Undergr Space Technol* 118:104190
- Lü Q, Low BK (2011) Probabilistic analysis of underground rock excavations using response surface method and SORM. *Comput Geotech* 38(8):1008–1021
- Lü Q, Xiao Z, Zheng J, Shang Y (2018) Probabilistic assessment of tunnel convergence considering spatial variability in rock mass properties using interpolated autocorrelation and response surface method. *Geosci Front* 9(6):1619–1629
- Luo WJ, Yang XL (2018) 3D stability of shallow cavity roof with arbitrary profile under influence of pore water pressure. *Geomech Eng* 16(6):569–575
- Michalowski RL, Park D (2020) Stability assessment of slopes in rock governed by the Hoek–Brown strength criterion. *Int J Rock Mech Min Sci* 127:104217
- Mollon G, Dias D, Soubra AH (2009) Face stability analysis of circular tunnels driven by a pressurized shield. *J Geotech Geoenviron Eng* 136(1):215–229



- Mollon G, Dias D, Soubra AH (2011a) Rotational failure mechanisms for the face stability analysis of tunnels driven by a pressurized shield. *Int J Numer Anal Meth Geomech* 35(12):1363–1388
- Mollon G, Dias D, Soubra AH (2011b) Probabilistic analysis of pressurized tunnels against face stability using collocation-based stochastic response surface method. *J Geotech Geoenviron Eng* 137(4):385–397
- Pan Q, Dias D (2017) Probabilistic evaluation of tunnel face stability in spatially random soils using sparse polynomial chaos expansion with global sensitivity analysis. *Acta Geotech* 12(6):1415–1429
- Pan Q, Dias D (2018) Probabilistic analysis of a rock tunnel face using polynomial chaos expansion method. *Int J Geomech* 18(4):04018013
- Pan Q, Dias D, Sun Z (2017) A new approach for incorporating Hoek–Brown failure criterion in kinematic approach—case of a rock slope. *Int J Struct Stab Dyn* 17(7):1771008
- Phoon KK, Huang SP (2007) Uncertainty quantification using multi-dimensional Hermite polynomials. *Probab Appl Geotech Eng* 1–10
- Phoon KK, Ching J (2014) Risk and reliability in geotechnical engineering. CRC Press, Boca Raton
- Renani HR, Martin CD (2020) Slope stability analysis using equivalent Mohr–Coulomb and Hoek–Brown criteria. *Rock Mech Rock Eng* 53(1):13–21
- Saada Z, Maghous S, Garnier D (2013) Pseudo-static analysis of tunnel face stability using the generalized Hoek–Brown strength criterion. *Int J Numer Anal Meth Geomech* 37(18):3194–3212
- Sari M, Karpuz C, Ayday C (2010) Estimating rock mass properties using Monte Carlo simulation: Ankara andesites. *Comput Geosci* 36(7):959–969
- Senent S, Mollon G, Jimenez R (2013) Tunnel face stability in heavily fractured rock masses that follow the Hoek–Brown failure criterion. *Int J Rock Mech Min Sci* 60:440–451
- Shen J, Karakus M (2014) Simplified method for estimating the Hoek–Brown constant for intact rocks. *J Geotech Geoenviron Eng* 140(6):04014025
- Shokri S, Shademan M, Rezvani M, Javankhoshdel S, Cami B, Yacoub T (2019) A review study about spatial correlation measurement in rock mass. In: *Rock Mechanics for Natural Resources and Infrastructure Development-Full Papers: Proceedings of the 14th International Congress on Rock Mechanics and Rock Engineering*, Foz do Iguassu, Brazil. CRC Press
- Song KI, Cho GC, Lee SW (2011) Effects of spatially variable weathered rock properties on tunnel behavior. *Probab Eng Mech* 26(3):413–426
- Sow D, Carvajal C, Breul P, Peyras L, Rivard P, Bacconnet C (2017) Modeling the spatial variability of the shear strength of discontinuities of rock masses: application to a dam rock mass. *Eng Geol* 220:133–143
- Su L, Wan HP, Li Y, Ling XZ (2018) Soil-pile-quay wall system with liquefaction-induced lateral spreading: experimental investigation, numerical simulation, and global sensitivity analysis. *J Geotech Geoenviron Eng* 144(11):04018087
- Sun Z, Li J, Pan Q, Dias D, Li S, Hou C (2018) Discrete kinematic mechanism for nonhomogeneous slopes and its application. *Int J Geomech* 18(12):04018171
- Xu J, Wang D (2019) Structural reliability analysis based on polynomial chaos, Voronoi cells and dimension reduction technique. *Reliab Eng Syst Saf* 185:329–340
- Yang XL, Huang F (2011) Collapse mechanism of shallow tunnel based on nonlinear Hoek–Brown failure criterion. *Tunn Undergr Space Technol* 26(6):686–691
- Yang XL, Wang JM (2011) Ground movement prediction for tunnels using simplified procedure. *Tunn Undergr Space Technol* 26(3):462–471
- Yang XL, Yin JH (2004) Slope stability analysis with nonlinear failure criterion. *J Eng Mech* 130(3):267–273
- Yang XL, Yin JH (2010) Slope equivalent Mohr–Coulomb strength parameters for rock masses satisfying the Hoek–Brown criterion. *Rock Mech Rock Eng* 43(4):505–511
- Zeng P, Senent S, Jimenez R (2016) Reliability analysis of circular tunnel face stability obeying Hoek–Brown failure criterion considering different distribution types and correlation structures. *J Comput Civ Eng* 30(1):04014126
- Zhang W, Goh ATC (2012) Reliability assessment on ultimate and serviceability limit states and determination of critical factor of safety for underground rock caverns. *Tunn Undergr Space Technol* 32:221–230

**Publisher's Note** Springer Nature remains neutral with regard to jurisdictional claims in published maps and institutional affiliations.